



The effect of copper doping on the structural, optical, and electrical properties of nickel oxide thin films for optoelectronic applications

Ban K. Mohammed¹ · Mustafa K. A. Mohammed² · Duha S. Ahmed¹

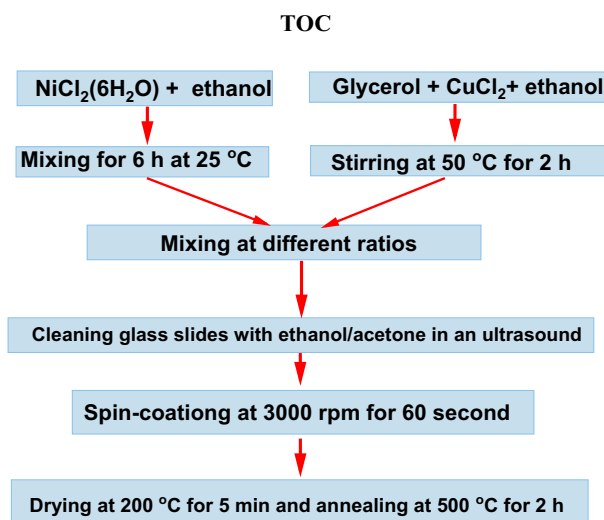
Received: 28 December 2020 / Accepted: 15 April 2021 / Published online: 7 May 2021

© The Author(s), under exclusive licence to Springer Science+Business Media, LLC, part of Springer Nature 2021

Abstract

In this paper, structural, optical, and electrical features of undoped and copper-incorporated nickel oxide (Cu/NiO) films with different mole ratios (0.01, 0.05, 0.1%) were studied. The prepared Cu/NiO films with a thickness of 100 nm were deposited on glass substrates using sol–gel combined with a spin coating technique. The results of X-ray diffraction (XRD) showed that all Cu/NiO films are polycrystalline of a cubic phase with a sharp tip predominating in the (111) direction. The estimated crystallite sizes of the prepared films were found in the range of nanoscale dimensions (19.115, 21.924, 23.057, 26.219 nm) by employing XRD data. Besides, images of the atomic force microscopy (AFM) and scanning electron microscope (SEM) reveal that the surfaces of the Cu-doped NiO films are smooth, holes-free, cracks-free, and homogeneous with dense fullness. Fourier transform infrared (FTIR) findings demonstrated that the emergence of the two chemical bonds located at 400–500 cm^{-1} attributed to Ni–O stretching vibration. However, the results did not show any evidence about the emergence of the Cu–O bond due to the weak copper concentration in the samples. Moreover, prepared films showed high optical transparency (94%) in the range of visible region and decreased to 92% with an addition of 0.1% Cu, which confirms the possibility of using them as window layers in solar cells. Finally, the electrical measurements showed that the surface resistance of NiO film decreased significantly after Cu doping. Our results could pave a good opportunity for providing insight into Cu-doped NiO properties and their usage in optoelectronic applications.

Graphical Abstract



✉ Mustafa K. A. Mohammed
mustafa_kareem97@yahoo.com

² Computer Sciences Department, Dijlah University College, Al-Masafi Street, Al-Dora, Baghdad 00964, Iraq

¹ Branch of Applied Physics, Department of Applied Sciences, University of Technology, Baghdad 100001, Iraq

Keywords Nickel oxide · Spin-coating · Copper doping · Optical properties · Morphology

Highlights

- Cu-doped NiO thin films with different Cu additives (0.01, 0.05, 0.1%) were prepared using a facile spin-coating method.
- NiCl₂ (6H₂O) salt and CuCl₂ precursors were used to fabricate Cu-doped NiO solution using a sol–gel process.
- The Cu additive lets improve the crystallinity of NiO film with a larger crystallite size.
- The prepared Cu–NiO films showed low surface roughness with high optical transparency and electrical conductivity.

1 Introduction

Nickel oxide (NiO) is a p-type semiconducting material with a direct and wide bandgap (E_g) in the range of 3.6–4 eV and its crystal structure is similar to that of sodium chloride [1–3]. NiO has gained considerable attention for different applications such as solar cell [4], photodetector [5], gas sensor [6], light-emitting diode [7], anticancer activity [8], antimicrobial activity [9], water treatment [10], and so on. As reported in the literature, the use of transition metal as an additive (for example gold, silver, copper, etc.) is an effective approach for improving semiconductor merits [11–14]. The benefit of employing metal additives in the NiO structure is attributed to the production of thin films with enhanced crystallinity, morphology, and electrical conductivity [15–17]. Pristine NiO reveals poor optical merits, which are developed from defects like interstitial Ni or O₂ vacancy. This drawback limits the use of NiO films directly in most applications. Incorporating metals into NiO can be used for tuning optical properties [18–20]. Besides, it is difficult to acquire visible light absorption on an undoped NiO film [21]. Cu has been widely reported as an efficient additive for tuning E_g of thin films for use in optoelectronic applications [22–25]. In this regard, NiO thin films can be prepared through diverse approaches such as hydrothermal [26], sputtering [27], chemical vapor deposition [28], pulsed laser deposition [29], and chemical bath deposition [30]. Among all these methods, sol–gel spin-coating technique has been used to deposit polycrystalline NiO due to its features, including low-temperature processing, potential usage of high-purity starting precursors, low cost, and facile process without any vacuum equipment [31]. Sahoo et al. employed a spin-coating process for high doping of Cu (5%) into NiO films and they found that the Cu additive improved absorbance and electrical conductance of NiO films [32]. The same concentration was also used in the study reported by Kyung and coworkers, where NiO layers were doped with 5% Cu additive using a solution-processed sol–gel method for enhancing NiO properties [33]. The decrease in the bandgap energy and resistivity was observed in this study with improved crystallinity. Barir et al. reported the effects of precursor concentration on NiO films by depositing on heated glass substrates using a spray pyrolysis method [34].

An increment in NiO crystallite size over 37.04 nm was obtained using 0.1 M content of Cu. Recently, Tuba also introduced Cu dopants with different amounts into NiO films successive ionic layer absorption and reaction (SILAR) [35]. The crystallinity of the deposited films significantly enhanced with an increase in the grain size. Recently, Seon and coworkers used (10-mol%) of Cu as a dopant into the NiO layer for enhancing the electrical conductivity and electrochemical activity [36]. In this context, it is worth noting that further investigations and discussion need to be elucidated. As we stated above, previous works used high concentration Cu additive, so in this study, we try to improve the properties of NiO thin films using a low concentration of Cu additive. The main goal of our paper is to enhance NiO film at low Cu additive for optoelectronic applications, where merits, such as good crystallinity, high transparency, high electrical conductivity are important for this field. Here we used sol–gel spin-coating method for preparing undoped and Cu-doped NiO films and systematically comparing these films. Most importantly, the impacts of Cu incorporating NiO structure were investigated and discussed. By using Cu as an additive, the optical, structural, morphological, and electrical merits of the prepared NiO layer were improved.

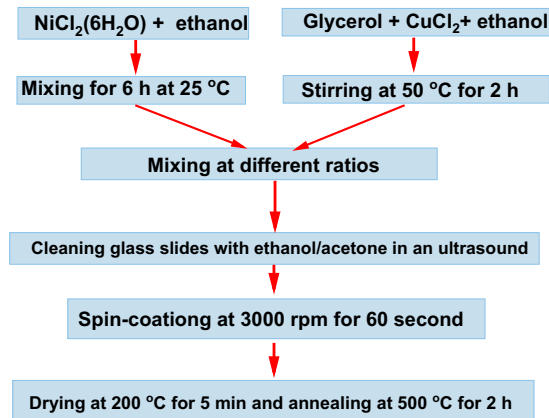
2 Experimental part

2.1 Solution preparation

The sol–gel method was utilized to synthesize undoped and Cu-doped NiO films with diverse molar ratios. To prepare a solution of nickel chloride salt (NiCl₂ (6H₂O), Sigma-Aldrich), the 0.4 M molarity (9.5 g) of NiCl₂ (6H₂O) was dissolved in 100-ml ethanol (99%, Merck) and stirred slowly for six hours at room temperature using a magnetic stirrer, to ensure that no precipitate and the material dissolve in ethanol. Then, to obtain a homogeneous green solution, 2 ml of glycerol (Sigma-Aldrich) was dissolved in 20 ml of ethanol using a magnetic stirrer, then mixed with 0.01 M of copper chloride (CuCl₂, Merck) at 10% (V/V) by stirring at 50 °C for 2 h before deposition. To obtain the NiO/Cu solutions, the NiCl₂ (6H₂O) solution was mixed with different volume ratios of the CuCl₂ mixture, as summarized in Table 1.

Table 1 The volumes taken from the copper ions added to the nickel ion to obtain the molar ratios required for film preparation

Rank	NiCl ₂ (6H ₂ O) 0.4 M (ml)	CuCl ₂ 0.01 M (ml)	NiO:Cu (mol%)
1	5	0.02	0.01
2	5	0.1	0.05
3	5	0.2	0.1

**Fig. 1** Schematic diagram showing the experimental steps of this work

2.2 Deposition of the thin films

Glass slides (Sigma-Aldrich) with 1 cm × 1 cm were cleaned with an ultrasonic bath of distilled water, ethanol, and acetone successively for 10 min and dried at 40 °C for 5 min. A volume of 100 μl from the solution was selected for the film deposition conditions. The prepared solution was poured as droplets on glass slides at room temperature and spin-coated for 60 s at 3000 rpm. Then, the deposited films were exposed to a temperature of 200 °C for 5 min to eliminate the volatile solvent by heat. After that, samples were placed in a Jinyu-700 electric furnace for annealing at 500 °C for 2 h. Figure 1 shows a diagram of the steps for preparing Cu-doped NiO films from their solutions.

2.3 Characterization

The thicknesses of the NiO films were measured using an optical thin film measurement (Lambda LIMF-10) system and the values were found to be about 100 nm. Ultraviolet–visible spectroscopy (UV–Vis) was used to record the optical characteristics of films using Ocean Optics (CHEM2000-UV-VIS). The structural properties of films were conducted by the X-ray diffraction (XRD) technique with Cu_{Kα} (λ = 1.54050 Å) irradiation operated at 40 kV and 30 mA and (Shimadzu XRD-6100/7000 X-ray diffractometers). The morphology of films was investigated

using a scanning electron microscope (SEM) (VEGA3). The topography of films was characterized via atomic force microscopy (AFM) (Bruker, CSPM-AA3000). The Fourier transform infrared (FTIR) spectra of samples were obtained using a Burker (IFS-125HR) device with a KBr disc.

3 Results and discussion

Figure 2 shows the XRD spectrum of the NiO films doped with different ratios of Cu. Bragg's reflections are observed at the angles 2θ of 37.43° and 43.23°, which can be ascribed to (111) and (200) planes, respectively. The XRD findings in this work agree with previous studies [3, 8, 33, 34]. From XRD data, important parameters such as the interlayer distance (*d*), lattice constant (*a*), the crystallite size (*D*), and dislocation density (*δ*) can be evaluated using the following equations [37–40]:

$$n\lambda = 2d_{hkl} \sin\theta \quad (1)$$

$$d_{hkl} = \frac{a}{\sqrt{h^2 + k^2 + l^2}} \quad (2)$$

$$D = \frac{0.94 \lambda}{\beta \cos\theta} \quad (3)$$

$$\delta = \frac{1}{D^2} \quad (4)$$

Where the *n*, *λ*, *θ*, *hkl*, *β* are diffraction order, the wavelength of X-ray, diffraction angle, Miller indices, and the width of the curve: radian at mid-maximum intensity (FWHM) taken from highest (111) peak of X-ray spectrum of NiO film, respectively. By comparing the *d_{hkl}* values with the standard JCPDS (4-0835 card), ensure that the films have a cubic structure. Also, the value of the lattice constant was found to be equal to 0.4171 nm, which is almost equal to the standard JCPDS value (0.4176 nm). X-ray spectra of Cu-modified NiO films with molar proportions of 0.01, 0.05, and 0.1% have peaks observed at the angles of 37.32° and 43.09° for a ratio of 0.01% and 37.40°, 43.56° for a ratio of 0.05%, while 37.31° and 43.31° for a ratio of 0.1%. Moreover, the values of the intersections between the reflective surfaces *d_{hkl}* and the corresponding values of the mentioned angles are equal to 0.2419, 0.2444, and 0.2407 nm, respectively. Where it can be inferred that the NiO is polycrystalline, have a cubic phase, and that the values of reflectivity exhibit a high degree of crystallinity with a sharp tip predominant in the directional (111) as well. The XRD spectra did not show the birth of new phases that are attributed to diffraction peaks, and that a change in the average crystallite size and density of dislocations was observed with the change of doping ratios as indicated in Table 2. The undoped NiO shows weak

Fig. 2 X-ray diffraction spectra of undoped and Cu-doped NiO films

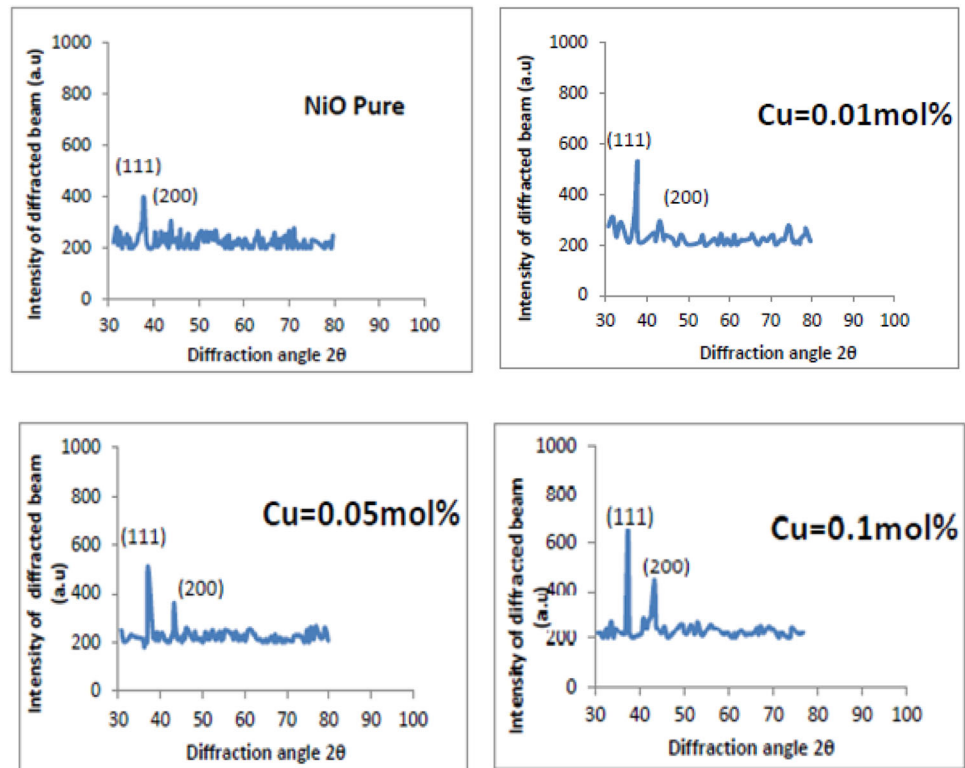


Table 2 Structural properties of undoped and Cu-doped NiO films

Sample	Crystallite size (nm)	Lattice constant (nm)	Dislocation density $\times 10^{-11}$ (line/cm ²)
NiO	19.215	0.4092	2.702702
NiO:0.01 mol% Cu	21.924	0.4183	2.083333
NiO:0.05 mol% Cu	26.219	0.4233	1.454545
NiO:0.1 mol% Cu	23.057	0.4167	1.881024

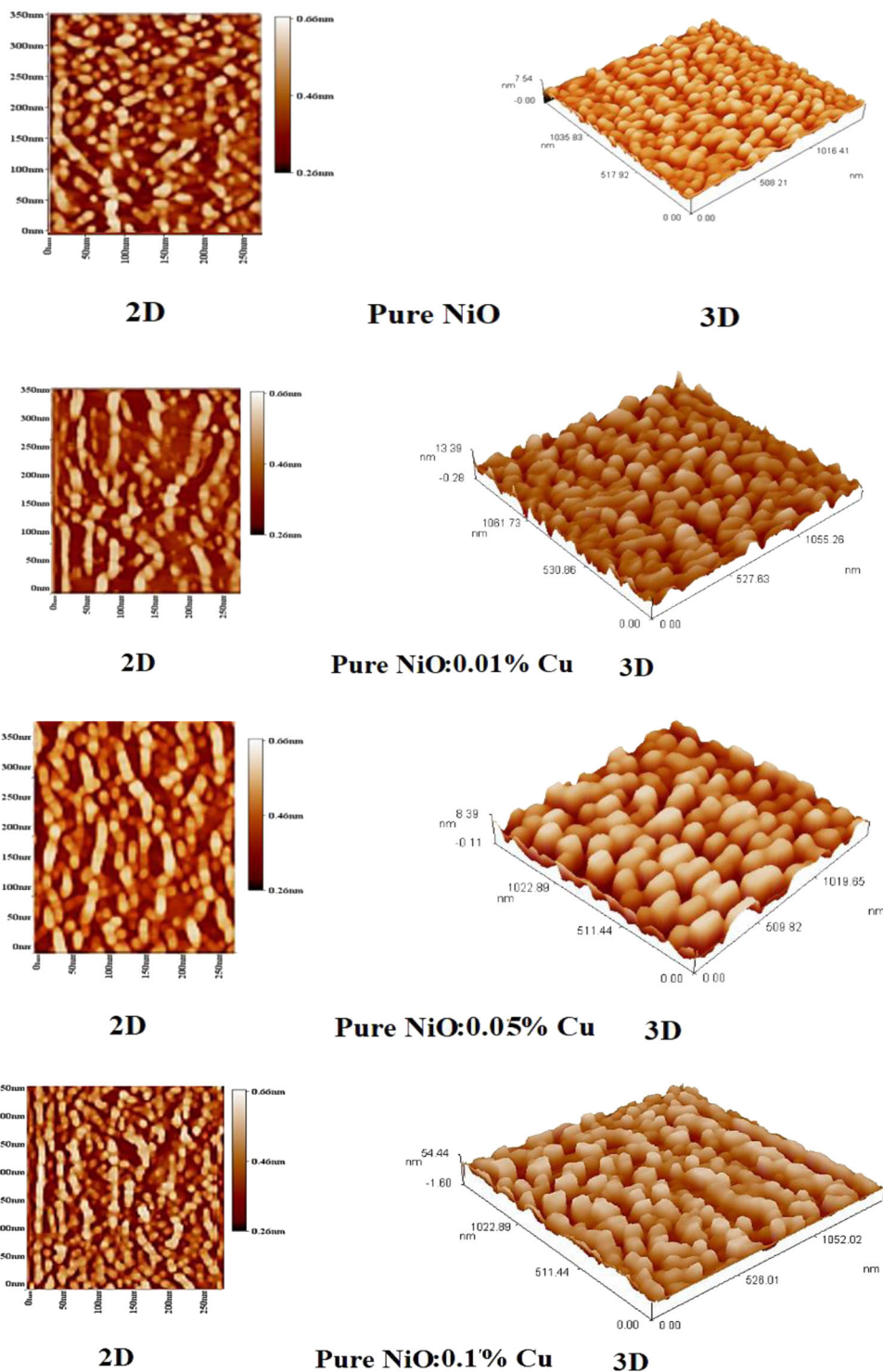
(111) and noisy (200) peaks, which indicates that the poor crystallinity of the film. This may be due to the incomplete formation of the NiO film at this process. With increasing precursor concentration from 0.01 to 0.1%, the improvement of crystallization was observed. It is also noticed that the intensity of the (111) diffraction peak of the papered film progressively enhanced and the full width at half maximum of the peak narrowed relative to that of the undoped NiO, implying better crystal quality [36].

The surface topography of the undoped and Cu-doped NiO layers deposited on glass bases was examined using AFM at room temperature. AFM images are shown in Fig. 3, which represents images of film surfaces in two dimensions (2D) and three dimensions (3D), with a magnification of 10^8 times. The films have smooth and a homogeneous surface in, which the distribution of crystalline grains is uniform and has their fullness is airtight without cracks and holes, which indicates good adhesion of the films to the glasses. The surface roughness of the examined film models

increased slightly with the increase in the doping ratios in the case of copper (Table 3). This agrees well with the results obtained by other researchers [1–3]. This may be attributed to the large ionic radius of the copper, which results in a deformed state of the crystal lattice. In addition, the RMS roughness of NiO film increases as Cu doping in it increases from 0.01 to 0.1% owing to its enlarged crystalline size. NiO and Cu-doped NiO thin films can be examined at the nano dimension and surface roughness values also obtained. We can conclude that no. of Ni^{2+} vacancies increase with increasing doping concentration [35].

To study the shape of the film surface and to know the effect of the doping ratio of Cu additive, the SEM technique was used. Figure 4 displays SEM images of undoped and Cu-doped NiO thin films with various weights. As seen, the images showed that the undoped and Cu doped NiO films had homogeneous, smooth, clear, and dense fullness surfaces, without cracks or holes, indicating that films have good adhesion. By increasing the percentage of Cu doping,

Fig. 3 AFM images of undoped and Cu-doped NiO films



we observe a significant increase in the distributed particles on the surface of NiO film. Figure 5 shows the distribution of particles obtained by ImageJ software to qualitative reveal SEM images (Table 4).

In this study, the absorption frequency that characterizes the type of vibration of a particular bond such as Ni–O and

Cu–O was investigated. Therefore, we will use this characteristic by scanning the field of wavelengths in the range $4000\text{--}400\text{ cm}^{-1}$, the chemical bonds are determined, as revealed in Fig. 6. By determining the vibration locations in the infrared spectrum, we concluded the chemical bond (Ni–O) and observed that the absorption peak of the NiO

bond appears in the permeability curve for undoped samples with a frequency of 451 cm^{-1} , which is consistent with the reference [30]. By comparing the curve of the doped samples with the curve of the undoped samples, we notice a great match between them in the values of the peaks, and the difference lies only in their strength, that is, the results did not show the permeability of the undoped samples anything new about the emergence of the Cu–O bond or not. This may be due to the weak copper concentration in the samples, which may enhance the peak of the latter. The band at 1050 cm^{-1} is attributed to C–O stretching vibration of epoxy groups, which originates from the reaction of the samples with CO_2 from the air during the analysis procedure [11]. The prominent band at 2930 cm^{-1} is typical of C–H symmetric stretching and carbon impurity in the samples.

Figure 7 shows the transmittance spectrum for glass and NiO films doped with different molar ratios in the wavelength range of 300–800 nm. The transmittance appears in two distinct regions, the first at short wavelengths less than 360 nm, where the transmittance increases almost suddenly with the

increase in the wavelength, and this is due to the beam-beam transmission. This arises from the high absorbance of the films in those regions. As for the second region, which is larger than 360 nm, we note that the transmittance of the film is higher, reaching (94%) within the visible region and continuing to the near-infrared region. This result is of great importance in solar cell applications, which surpasses the results of many researchers who have studied NiO compounds in the form of nano thickness and non-nano-thickness films deposited by a method similar to our study. At present, we find many researchers working to develop a solar cell conversion efficiency by reducing the losses resulting from several effects, including those related to the interaction of light with the cell material, i.e., the losses resulting from the optical characteristics of the cell. Also, by comparing the glass substrate with the prepared NiO films, we can see that the light loss in the visible range is very low, which is important for optoelectronic applications. The NiO film with 0.1% Cu additive showed the highest absorption compared with other films.

After the copper doping with the mentioned molar ratios, the transmittance values decreased to reach 92% when doped by 0.1 mol% within the visible region and continue into the near-infrared region. The decrease in the transmittance values with the increase in the impurity ratios may be attributed to the formation of localized levels of copper impurities within the energy gap. This is evident by decreasing the optical bandgap values for direct electronic transmissions [33]. The regularity of the curves in the transmittance spectra confirms the high homogeneity of the thicknesses in the deposited films by the method adopted in this paper.

Table 3 Results of AFM for undoped and Cu-doped NiO films

Ten-point height SZ (nm)	Root mean square Sq (nm)	Roughness average Sa (nm)	Mol % of Cu
23.9	6.06	5.24	0
20.8	5.13	4.47	0.01
65.3	11.30	9.87	0.05
30.2	14.00	10.70	0.1

Fig. 4 SEM images of undoped and Cu-doped NiO films (a) undoped, (b) 0.01%, (c) 0.05%, and (d) 0.1%

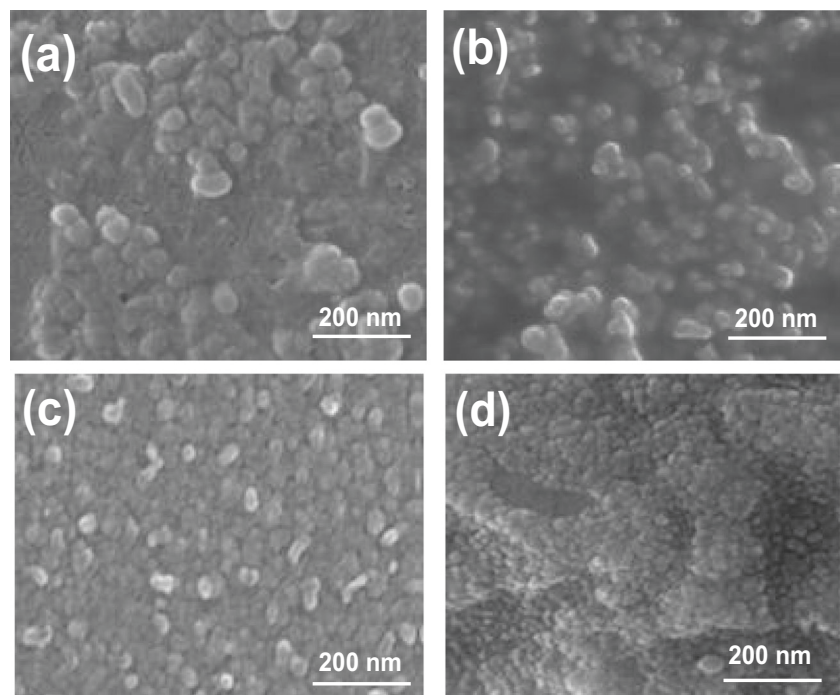


Fig. 5 Particle size distribution for prepared films. **a** Undoped NiO, **(b)** 0.01% Cu-doped NiO, **(c)** 0.05% Cu-doped NiO and **(d)** 0.1% Cu-doped NiO

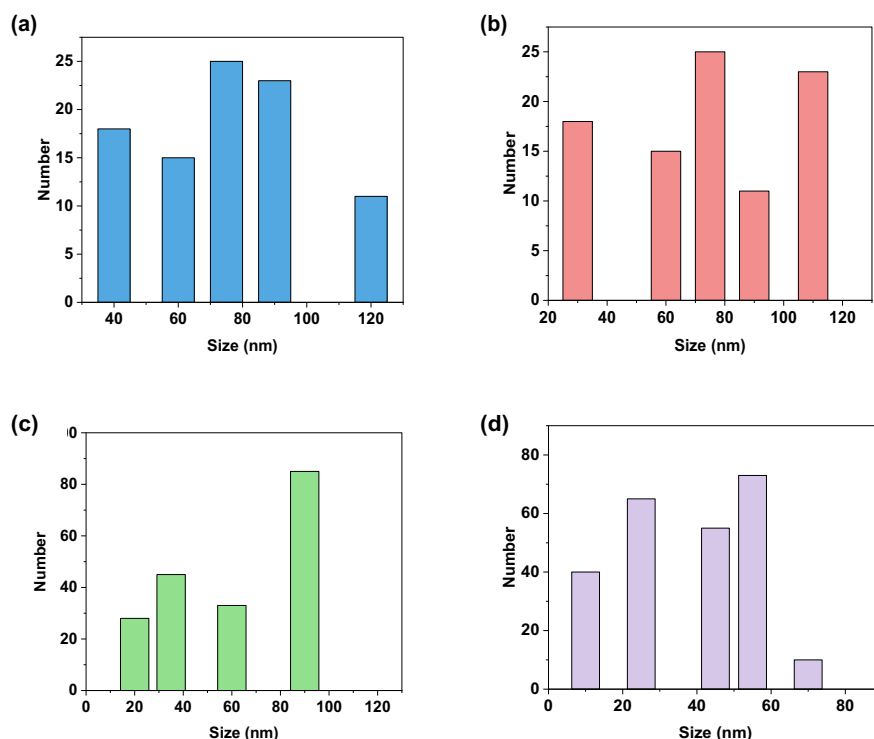


Table 4 Energy gap calculated from UV–visible spectra

Samples	Energy gap (eV)
Undoped	3.73
0.01%	3.61
0.05%	3.49
0.1%	3.42

Some optical properties such as absorption coefficient (α) and the E_g were calculated according to the following two equations [41–44]:

$$\alpha = 2.303A/t \quad (5)$$

$$ah\nu = \alpha_0 (h\nu - E_g)^r \quad (6)$$

Where t , A , r , ν , and h are the film thickness, absorbance, an exponential constant whose value depends on the transitions, the incident photon frequency, and the energy of the absorbed photon, respectively.

The direct energy gap value was obtained from the extension of the straight portion (tangent) of the results curve to cut the photon energy axis $h\nu$ at $(ah\nu)^2 = 0$ [42]. The permissible direct optical E_g value for the nano thickness NiO film was found to be 3.73 eV, which falls within the range of standard values of E_g (3.6–4 eV) (see Fig. 8). It was found that as the material is directed to nanoscale structures, the energy levels in the semiconductor become more discrete

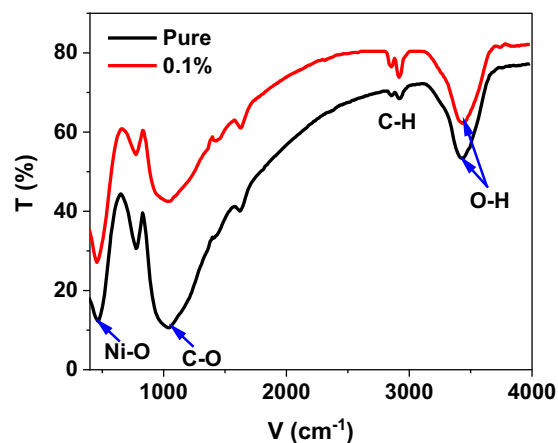


Fig. 6 FTIR spectra of undoped and imprinted NiO thin films

from each other, and the effective E_g increases. We note that the E_g values for the direct transmission gradually decrease with an increase in the doping and this is due to changes in the homogeneity of the local levels and their intensity, which increases with the increase of the Cu concentration in the precipitated films, i.e., increase charge carriers. The energy band gap values were decreased from 3.73 to 3.49 eV depending on the Cu concentration (Table 4). The optical absorption value of NiO thin films decreased as the percentage of Cu increased. This reduction in bandgap energy indicates that the crystal structure has improved, and the grain size increased [45–47].

It is well-known that the refractive index contains valuable information for higher efficiency optical materials and is considered an important parameter for optical materials design because it is closely related to the electronic polarization of ions and the local field within the material. The complex refractive index (N) can be expressed as follow [48]:

$$N = n - ik \tag{7}$$

where (n) and (k) are the real and imaginary parts of the refractive index, respectively, and can be calculated using the reflectance (R) of the film from the following relations [48]:

$$R = \frac{(n - 1)^2 + k^2}{(n + 1)^2 + k^2} \tag{8}$$

$$n = \left(\frac{1 + R}{1 - R} \right) + \sqrt{\frac{4R}{(1 - R)^2} - k^2} \tag{9}$$

$$k = \frac{\alpha\lambda}{4\pi} \tag{10}$$

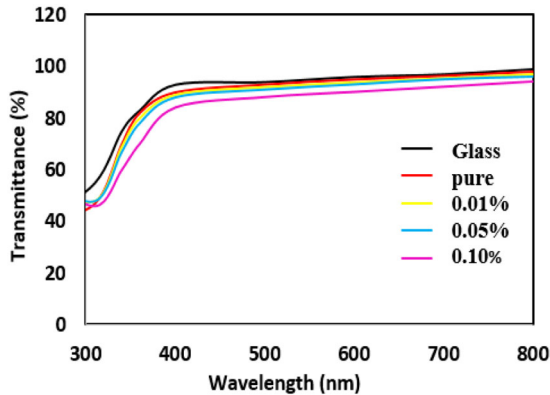


Fig. 7 Transmittance spectra of the glass substrate and NiO films

Figure 9 shows the reflectance as a function of wavelength. It is obvious that the reflectance increases with increasing Cu doping level. Figure 10 represents the change in refractive index as a function of the photon energy of the undoped and doped NiO films. We note that the refractive index curve behavior of the Cu-doped NiO films increases with increasing photon energy. Antireflection coatings considered the most process used as windows in solar cells fabrications in order to minimize the reflection while maximizing the transmission of light. From (Fig. 8), it was found that the variation of energy optical gap with doping concentration has a similar behavior compared to the refractive index (Fig. 10).

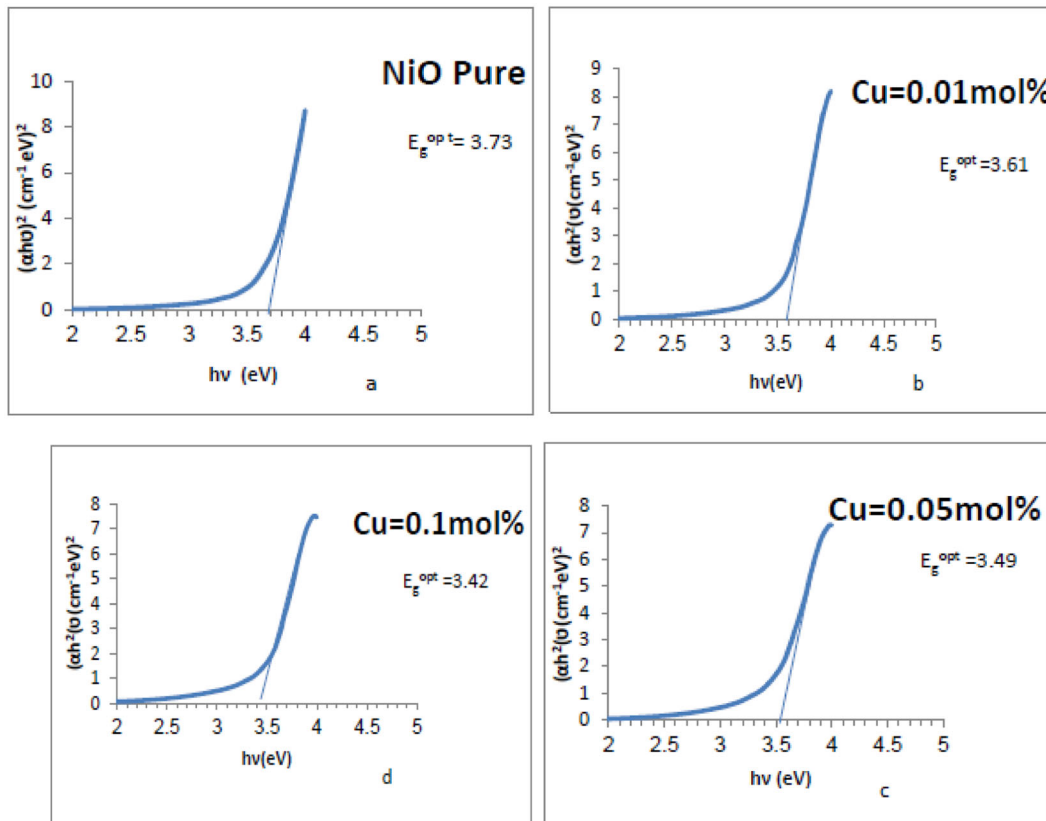


Fig. 8 Allowed direct E_g of undoped and Cu-doped NiO films

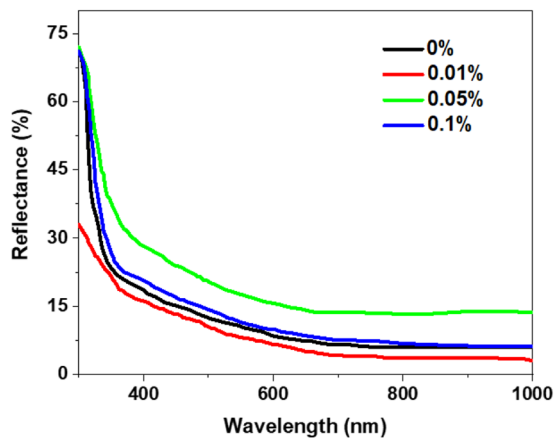


Fig. 9 Reflectance as a function of wavelength for pure and doped NiO thin films for different concentrations

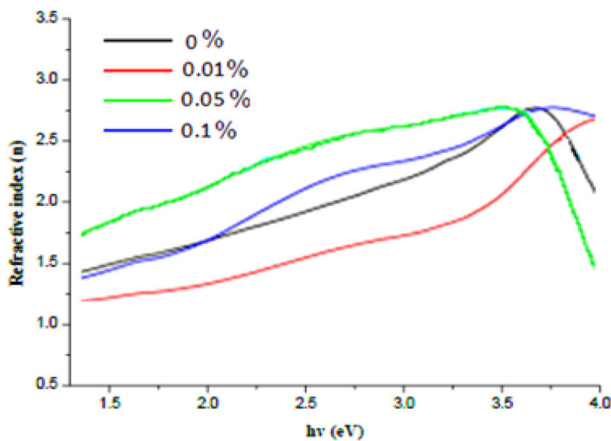


Fig. 10 Refractive index of undoped nickel oxide and copper-doped films

The surface resistance (R_s) values were measured using the four probes based on potential difference and electric current measurements of NiO films. Conductivity (σ) is the most important electrical properties and determined [49]:

$$\sigma = \frac{1}{\rho} = \frac{1}{R_s d} \tag{11}$$

Where d is a measured distance over cross-section area and R_s is the resistance of films. Figure 11 shows the changes in the values of both σ and surface resistance (R_s) in terms of Cu-doping ratios to NiO films. We note that the decrease in surface resistance increased the electrical conductivity, as the doping ratios increased, and this can be explained by the fact that Cu doping increased the charge carriers (Table 5). The highest conductivity in 0.01 and 0.1% films annealed at 500 °C may be due to the improvement of the carries excitations to conduction band as a result of bandgap narrowing, similar finding is reported by Qun et al. [50].

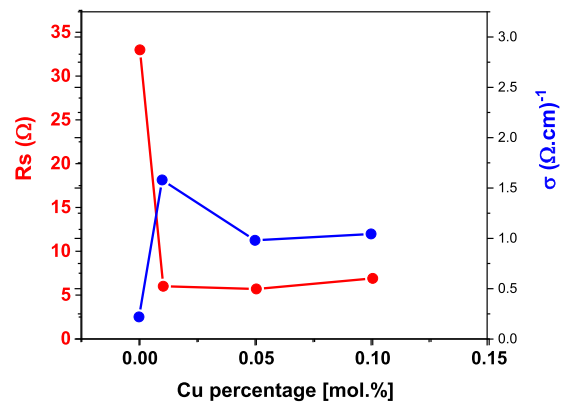


Fig. 11 changes in the values of both the surface resistance (R_s) and electrical conductivity (σ) as a function of the doping ratios of the films (Cu/NiO)

Table 5 Summary of the results of measurements (R_s) and (σ) using the four probes technique

Cu (%)	$R_s (\Omega) 10^4$	$\sigma (\text{cm } \Omega)^{-1}$
0	33.392721	0.214
0.01	6.055702	1.588
0.05	5.732162	0.980
0.1	6.990669	1.044

The values of the real dielectric constants were calculated from the equation [51]:

$$\epsilon_1 = n^2 - k^2 \tag{12}$$

Figure 12a shows the relationship between the real dielectric constant and the wavelength, where we notice the similarity of its behavior with the behavior of the refractive index in terms of the shape of the curve and the movement of its higher values toward higher wavelengths and these results from the dependence of the values of the real dielectric constant on the refractive index. We can estimate the imaginary part of the dielectric constant from the following relationship [51]:

$$\epsilon_2 = 2nk \tag{13}$$

And drawing it as a function of the photon energy, as in Fig. 12b, we notice the similarity of its curves with the curves of the refractive index, and this is also a result of the close relationship and its great influence on its values.

Finally, the comparison between this study and other related works is presented in Table 6. This comparison reveals the significant findings evaluated from this study compared with the literature. As we can see, the main significant difference between our work and other related

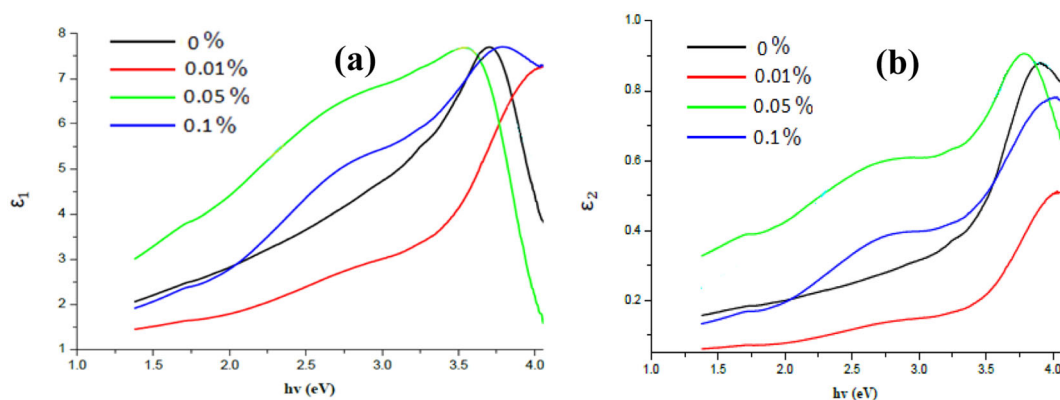


Fig. 12 **a** The change in the values of the real dielectric constant and **(b)** the change in the values of the imaginary dielectric constant as a function of the wavelength of the prepared films

Table 6 A comparison between our work and previous reports

Study	Ratio (%)	Crystallite size (nm)	Lattice constant	Roughness (nm)	Energy gap (eV)	σ (cm Ω) ⁻¹
Tuba et al. [35]	0.75	Not reported	Not reported	83.00	2.37	Not reported
Kyung et al. [33]	5.00	38.00	0.417	2.23	3.69	0.000434
Tithi et al. [23]	4.00	Not reported	Not reported	4.62	Not reported	Not reported
Pooja et al. [32]	5.00	Not reported	Not reported	Not reported	3.56	Not reported
Shweta et al. [22]	10.00	15.24	0.416	8.23	2.96	Not reported
This work	0.1	23.05	0.416	10.70	3.42	1.044000

works is the concentration of the optimized Cu additive. We used low concentration (0.1%) to improve the properties of the NiO films, while previous works used high concentrations. Furthermore, our study showed the nanocrystallite size of the prepared Cu-doped NiO film with a well-matched lattice constant, as reported in earlier works. The optimized Cu–NiO film revealed a wide energy gap with good electrical conductivity, which fulfills the requirements for optoelectronic applications.

4 Conclusions

In summary, the XRD results of NiO and Cu-doped NiO films with ratios of 0.01, 0.05, 0.1% showed that they are polycrystalline with a cubic phase and that the preferred orientation for crystalline grains is (111). The AFM images showed that the films have homogeneous and smooth surfaces in which the distribution of the grains is regular crystalline. The transmittance value of the NiO film is 94% within the visible region and continues into the near-infrared region. The transmittance of the prepared films was found to decrease with a small portion, which could be attributed to the low concentration of Cu additive. In this regard, the optical E_g of the NiO films was decreased from

3.73 for undoped NiO to 3.61, 3.49, and 3.42 eV for 0.01, 0.05, and 0.1% films, respectively. As for surface resistance, it experienced a clear decrease after vaccination, which increased the conductivity.

Compliance with ethical standards

Conflict of interest The authors declare no competing interests.

Publisher's note Springer Nature remains neutral with regard to jurisdictional claims in published maps and institutional affiliations.

References

- Zhou D, Xie D, Xia X, Wang X, Gu C, Tu J (2017) All-solid-state electrochromic devices based on WO₃/NiO films: material developments and future applications. *Sci China Chem* 60:3–12
- Da Rocha M, Rougier A (2016) Electrochromism of non-stoichiometric NiO thin film: as single layer and in full device. *Appl Phys A* 122:370
- R Alkarsifi, YA Avalos-Quiroz, P Perkhun, X Liu, M Fahlman, AK Bharwal, CM Ruiz, D Duche, J-J Simon, C Videlat-Ackermann, O Margeat, J Ackermann (2021) Organic–inorganic doped nickel oxide nanocrystals for hole transport layers in inverted polymer solar cells with color tuning. *Mater Chem Front* <https://doi.org/10.1039/D0QM00619J>

4. Lee H, Huang Y-T, Horn MW, Feng S-P (2018) Engineered optical and electrical performance of rf-sputtered undoped nickel oxide thin films for inverted perovskite solar cells. *Sci Rep* 8:5590
5. Zhang Y, Ji T, Zhang W, Guan G, Ren Q, Xu K, Huang X, Zou R, Hu J (2017) A self-powered broadband photodetector based on an n-Si(111)/p-NiO heterojunction with high photosensitivity and enhanced external quantum efficiency. *J Mater Chem C* 5:12520–12528
6. Zhao Y, Yan J, Huang Y, Lian J, Qiu J, Bao J, Cheng M, Xu H, Li H, Chen K (2018) Interfacial self-assembly of monolayer Mg-doped NiO honeycomb structured thin film with enhanced performance for gas sensing. *J Mater Sci Mater Electron* 29:11498–11508
7. Jung BO, Kwon YH, Seo DJ, Lee DS, Cho HK (2013) Ultraviolet light emitting diode based on p-NiO/n-ZnO nanowire heterojunction. *J Cryst Growth* 370:314–318
8. AlSalhi MS, Hammad M, Aziz MA, Fatima M, Shaheen F, Devanesana S, Farooq WA (2020) Synthesis of NiO nanoparticles and their evaluation for photodynamic therapy against HeLa cancer cells. *J King Saud Univ Sci* 32:1395–1402
9. Lalithambika KC, Thayumanavan A, Ravichandran K, Sriram S (2017) Photocatalytic and antibacterial activities of eco-friendly green synthesized ZnO and NiO nanoparticles. *J Mater Sci* 28:2062–2068
10. Sabouri Z, Akbari A, Hosseini HA, Hashemzadeh A, Darroudi M (2019) Bio-based synthesized NiO nanoparticles and evaluation of their cellular toxicity and wastewater treatment effects. *J Mol* 1191:101–109
11. Mustafa KAM (2020) Sol-gel synthesis of Au-doped TiO₂ supported SWCNT nanohybrid with visible-light-driven photocatalytic for high degradation performance toward methylene blue dye. *Optik* 223:165607
12. Mustafa KAM (2020) Carbon nanotubes loaded ZnO/Ag ternary nanohybrid with improved visible light photocatalytic activity and stability. *Optik* 217:164867
13. Mohammad MR, Ahmed DS, Mohammed MKA (2019) Synthesis of Ag-doped TiO₂ nanoparticles coated with carbon nanotubes by the sol-gel method and their antibacterial activities. *J Sol-Gel Sci Technol* 90:498–509
14. Ahmed DS, Mohammed MKA, Mohammad MR (2020) Sol-gel synthesis of Ag-doped titania-coated carbon nanotubes and study their biomedical applications. *Chem Pap* 74:197–208
15. Hameed MA, Ali OA, Al-Awadi SSM (2020) Optical properties of Ag-doped nickel oxide thin films prepared by pulsed-laser deposition technique. *Optik* 206:164352
16. Hotovy I, Huran J, Spiess L, Romanus H, Capone S, Rehacek V, Taurino AM, Donoval D, Siciliano P (2007) Au-NiO nanocrystalline thin films for sensor application. *J Phys* 61:435–439
17. Sangwaranatee N, Horprathum M, Chananonawathorn C, Hendro (2018) Effect of annealing treatment on sputtered copper oxide thin film. *Mater Today* 5:15170–15173
18. Shi J, Lai L, Zhang P, Li H, Qin Y, Gao Y, Luo L, Lu J (2016) Aluminum doped nickel oxide thin film with improved electrochromic performance from layered double hydroxides precursor in situ pyrolytic route. *J Solid State Chem* 241:1–8
19. Arunodaya J, Sahoo T (2020) Effect of Li doping on conductivity and band gap of nickel oxide thin film deposited by spin coating technique. *Mater Res Express* 7:016405
20. Awais M, Dowling DP, Decker F, Dini D (2015) Electrochemical characterization of nanoporous nickel oxide thin films spray-deposited onto indium-doped tin oxide for solar conversion scopes. *Adv Condens Matter Phys* 2015:1–18
21. Diao C-C, Huang C-Y, Yang C-F, Wu C-C (2020) Morphological, optical, and electrical properties of p-type nickel oxide thin films by nonvacuum deposition. *Nanomaterials* 10:636
22. Moghe S, Achary AD, Panda R, Shrivastava SB, Gangrade M, Shripathi T, Ganesan V (2012) Effect of copper doping on the change in the optical absorption behaviour in NiO thin films. *Renew Energy* 46:43–48
23. Sen T, Thangavel R, Nair UG (2017) Optical and electrical properties of copper doped nickel oxide thin films by using sol-gel spin coating method. *Mater Today Proc* 4:9597–9601
24. K Varunkumar, AS Ethiraj, A Kechiantz (2018) Optical absorption and thermal stability study of Cu doped NiO nanoparticles. *AIP Conf Proc* 1953:030174
25. Leyland NS, Podporska-Carroll J, Browne J, Hinder SJ, Quilty B, Pillai SC (2016) Highly efficient F, Cu doped TiO₂ anti-bacterial visible light active photocatalytic coatings to combat hospital-acquired infections. *Sci Rep* 6:24770
26. Brewster DA, Bian Y, Knowles KE (2020) Direct solvothermal synthesis of phase-pure colloidal NiO nanocrystals. *Chem Mater* 32(5):2004–2013
27. Sato K, Kim S, Komuro S, Zhao X (2016) Characteristics of Cu-doped amorphous NiO thin films formed by RF magnetron sputtering. *Jpn J Appl Phys* 55:06GJ10
28. Nigro RL, Battiato S, Greco G, Fiorenza P, Roccaforte F, Malandrino G (2014) Metal organic chemical vapor deposition of nickel oxide thin films for wide band gap device technology. *Thin Solid Films* 563(31):50–55
29. Gupta RK, Ghosh K, Kahol PK (2009) Fabrication and characterization of NiO/ZnO p-n junctions by pulsed laser deposition. *Physica E* 41:617–620
30. Gomaa MM, Boshta M, Farag BS, Osman MBS (2016) Structural and optical properties of nickel oxide thin films prepared by chemical bath deposition and by spray pyrolysis techniques. *J Mater Sci Mater Electron* 27(1):711–717
31. Iassi MJ, Sta I, Hajji M, Ezzaouia H (2014) Optical and electrical properties of nickel oxide thin films synthesized by sol-gel spin coating. *Mater Sci Semicond Process* 21:7–13
32. Sahoo P, Sharma A, Thangavel R (2019) Influence of Cu incorporation on physical properties of nickel oxide thin films synthesized by sol-gel method. *AIP Conf Proc* 2115:030621
33. Kim KH, Takahashi C, Abe Y, Kawamura M (2014) Effects of Cu doping on nickel oxide thin film prepared by sol-gel solution process. *Optik* 125:2899–2901
34. Barir R, Benhaoua B, Benhamida S, Rahal A, Sahraoui T, Gheriani R (2017) Effect of precursor concentration on structural optical and electrical properties of NiO thin films prepared by spray pyrolysis. *J Nanomater* 2017:10
35. Tuba ÇT (2020) Synthesis of copper-doped nickel oxide thin films: structural and optical studies. *Chem Phys Lett* 738:136884
36. Kim SY, Yun TY, Yu KS, Moon HC (2020) Reliable, high-performance electrochromic supercapacitors based on metal-doped nickel oxide. *ACS Appl Mater Interfaces* 12(46):51978–51986
37. Mohammed MKA (2020) High-performance hole conductor-free perovskite solar cell using a carbon nanotube counter electrode. *RSC Adv* 10:35831
38. Al-Mousoi AK, Mohammed MKA (2020) Engineered surface properties of MAPI using different antisolvents for hole transport layer-free perovskite solar cell (HTL-free PSC). *J Sol-Gel Sci Technol* 96:659–668
39. Mohammed MKA (2020) Studying the structural, morphological, optical, and electrical properties of CdS/PbS thin films for photovoltaic applications. *Plasmonics* 15:1989–1996
40. Mohammed MKA, Ahmed DS, Mohammad MR (2019) Studying antimicrobial activity of carbon nanotubes decorated with metal-doped ZnO hybrid materials. *Mater Res Express* 6:055404
41. Al-Mousoi AK, Mohammed MKA, Khalaf HA (2016) Preparing and characterization of indium arsenide (InAs) thin films by chemical spray pyrolysis (CSP) technique. *Optik* 127:5834–5840

42. Mohammed MKA, Al-Mousoi AK, Khalaf HA (2016) Deposition of multi-layer graphene (MLG) film on glass slid by flame synthesis technique. *Optik* 127:9848–9852
43. Jibrael RI, Mohammed MKA (2016) Production of graphene powder by electrochemical exfoliation of graphite electrodes immersed in aqueous solution. *Optik* 127:6384–6389
44. Mohammad RM, Duha SA, Mustafa KAM (2020) ZnO/Ag nanoparticles-decorated single-walled carbon nanotubes (SWCNTs) and their properties. *Surf Rev Lett* 27:1950123
45. I Manouchehri, D Mehrparvar, R Moradian, K Gholami, T Osati (2016) *Optik* 127: 8124–8129
46. T. Çayır Taşdemirci (2019) *Opt Quant Electron* 51: 245–253.
47. Mani Menaka S, Umadevi G, Manickam M (2017) *Mater Chem Phys* 191:181–187
48. Soyulu M, Yazici T (2017) CdO thin films based on the annealing temperature differences prepared by sol–gel method and their heterojunction devices. *Mater Res Express* 4:126307
49. Salih AT, Najim AA, Faisal AD (2020) Influence of annealing temperature on the structural, morphological, optical and electrical properties of Cu₇S₄ thin films prepared by chemical bath deposition. *J Inorg Organomet Polym Mater* 30:2258–2265
50. Li Q et al. (2017) Electronic modulation of electrocatalytically active center of Cu₇S₄ nanodisks by cobalt-doping for highly efficient oxygen evolution reaction. *ACS Nano* 11 (12):12230–12239
51. Abdullah MM (2020) Facile growth, physical characterization, and dielectric response of as-grown NiO nanostructures. *J King Saud Univ Sci* 32:1048–1054